Supporting information for

Structure and photoluminescence of Mn$^{2+/4+}$-activated doubly ordered spinel Mg$_4$(Ga/Al)SbO$_8$: site-selective Al^{3+}-to-Ga^{3+} substitution enabling Mn^{4+} accumulation, excellent anti-thermal quenching of Mn^{2+} green-emission, and optical thermometry

Zien Cheng,[a,#] Guangxiang Lu,[a,#] Yuxuan Qi,[b] Jinmei Huang,[a] Gonggui Yan,[a] Leiming Fang,[c] Maxim Avdeev,[*d,e] Tao Yang[*a] and Pengfei Jiang,[*a]

[a]College of Chemistry and Chemical Engineering, Chongqing University, Chongqing 401331, China

[b]Chongqing Academy of Metrology & Quality Inspection, Chongqing 401121, China

[c]Key Laboratory for Neutron Physics, Institute of Nuclear Physics and Chemistry, China Academy of Engineering Physics, Mianyang 621999, China

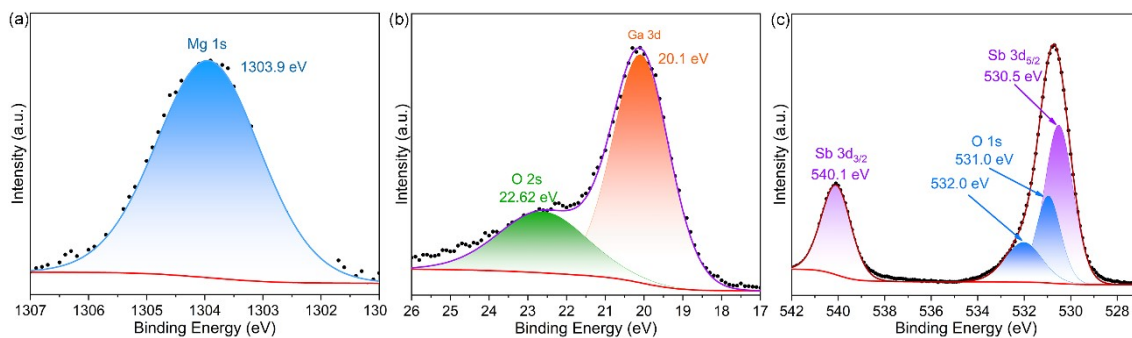[d]Australian Nuclear Science and Technology Organisation, Lucas Heights, NSW 2234, Australia

[e]School of Chemistry, The University of Sydney, Sydney, NSW 2006, Australia

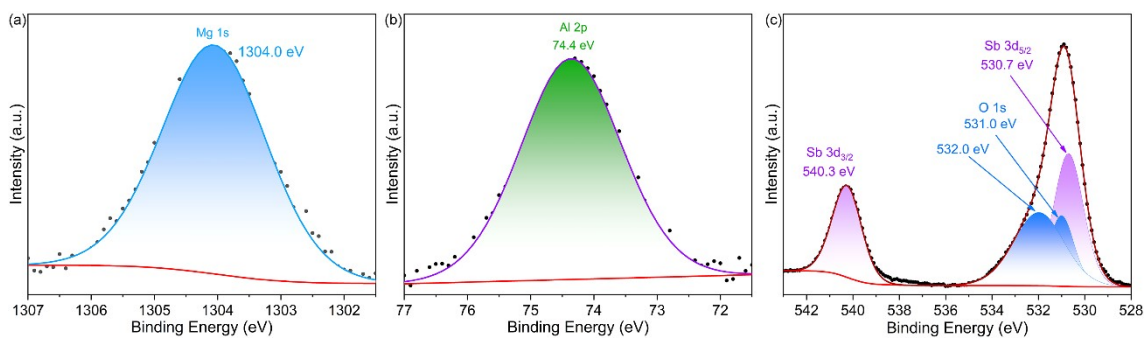*Corresponding Authors: max@ansto.gov.au; taoyang@cqu.edu.cn; pengfeijiang@cqu.edu.cn.

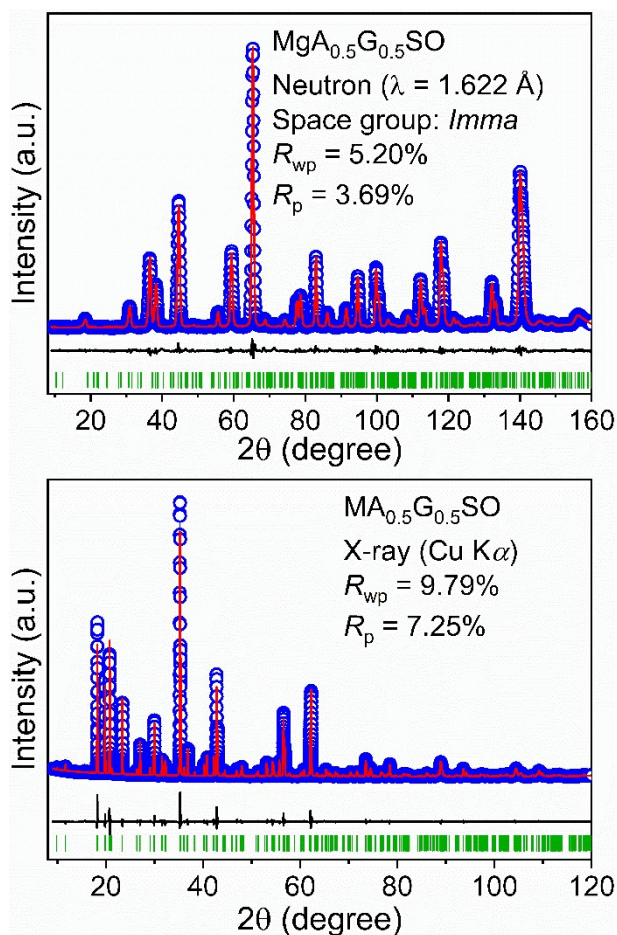[#]These authors contributed equally.
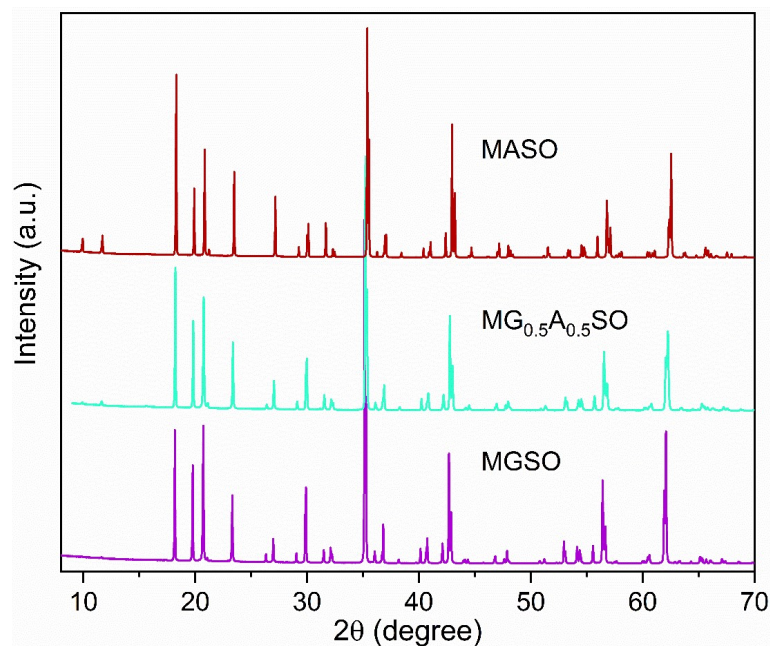
**Fig. S1** XRD patterns for MGSO, MG$_{0.5}$A$_{0.5}$O, MASO.

Fig. S2 High-resolution XPS spectra for Mg 1s (a), Ga 3d (b), and O 1s and Sb 3d (c).

Fig. S3 High-resolution XPS spectra for Mg 1s (a), Al 3d (b), and O 1s and Sb 3d (c).

Fig. S4 Rietveld refinement plots of NPD and PXRD data for $MG_{0.5}A_{0.5}SO$. The circles, red and black solid lines represent the observed data, calculated data, and their differences. The expected Bragg positions are given as green bars at the bottom of the patterns.
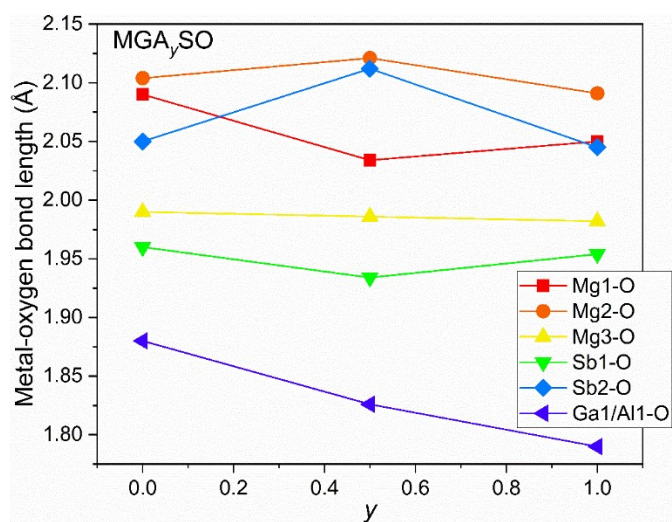
Fig. S5 Plots of metal−oxygen bond length as a function of Al-content in MGA_yO ($y = 0$, 0.5, 1).
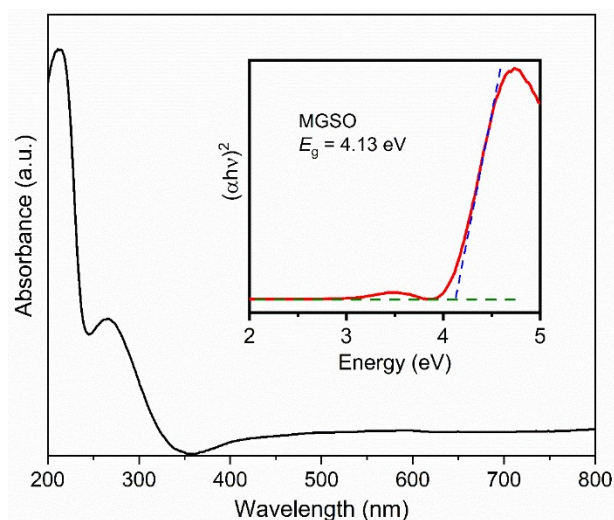
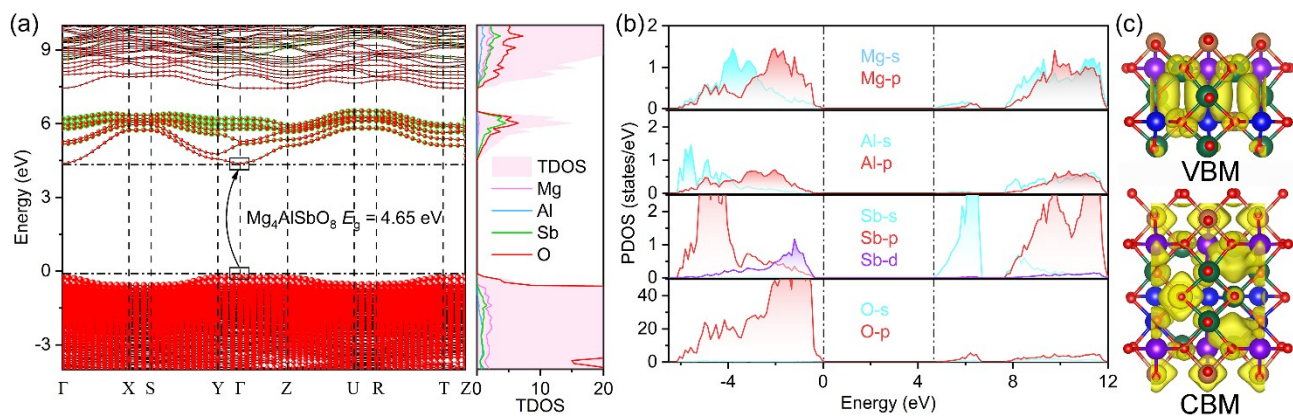**Fig. S6** UV−vis diffusion spectra for MGSO. The insets show the plots of $(\alpha h v)^2$ as a function of the photon energy.

Fig. S7 (a) Electronic band structure of MASO. (b) PDOS of Mg, Al, Sb, and O for MGSO. (c) Isosurfaces (5×10^{-4} e$^-$/bohr^3) of the partial charge density at the VBM and CBM of MASO.
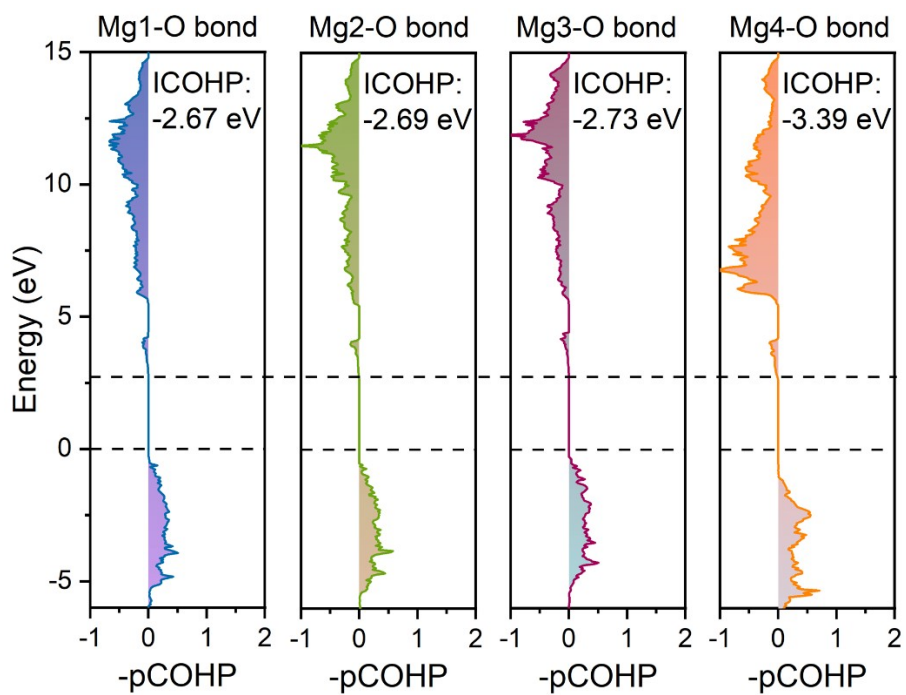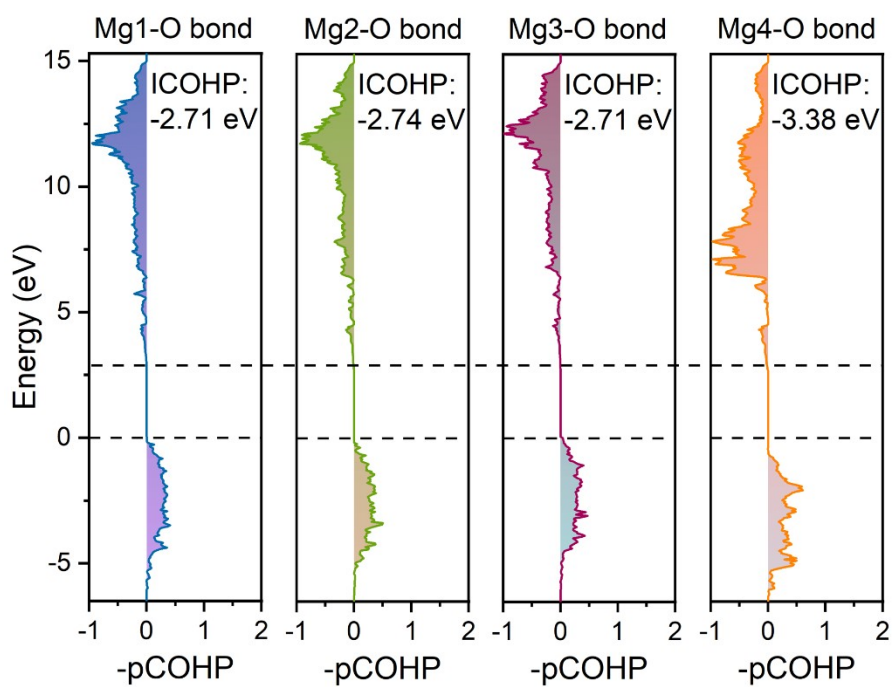
MGSO

MASO

Fig. S8 COHP diagrams of the Mg−O bonds in MGSO and MASO.
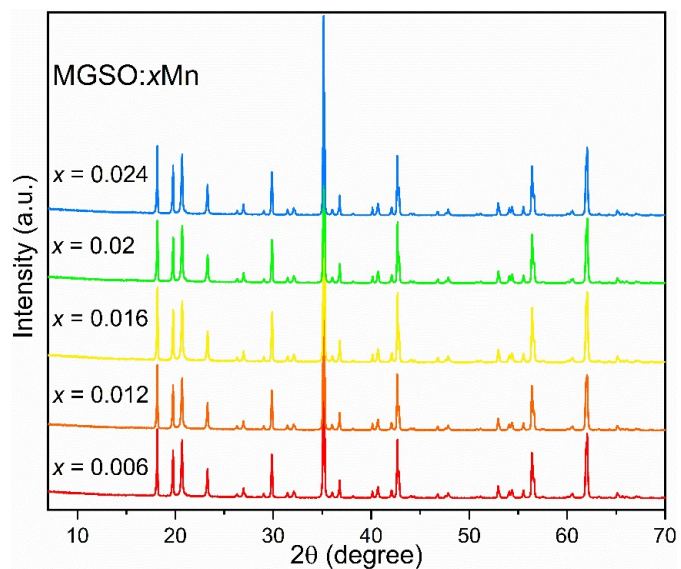
Fig. S9 XRPD patterns for MGSO:*x*Mn.
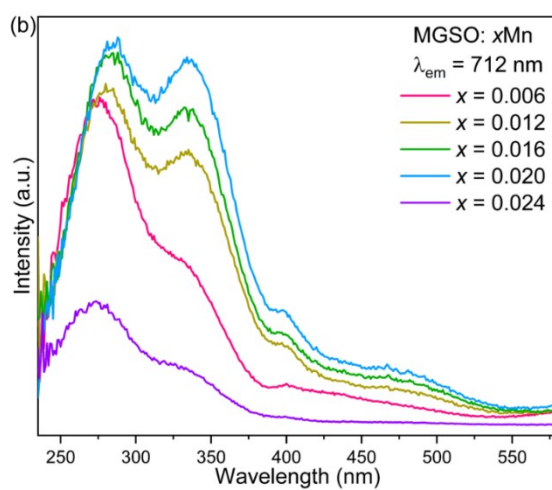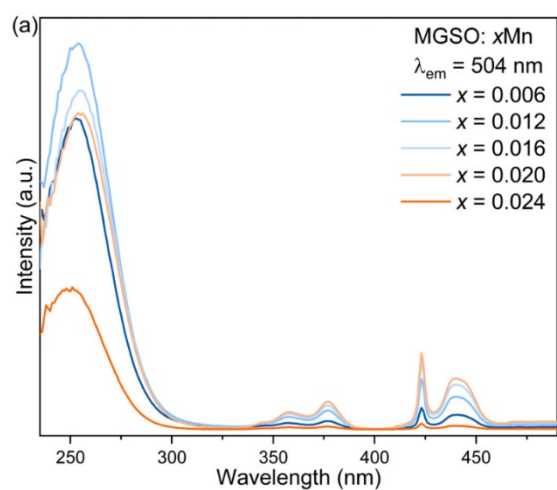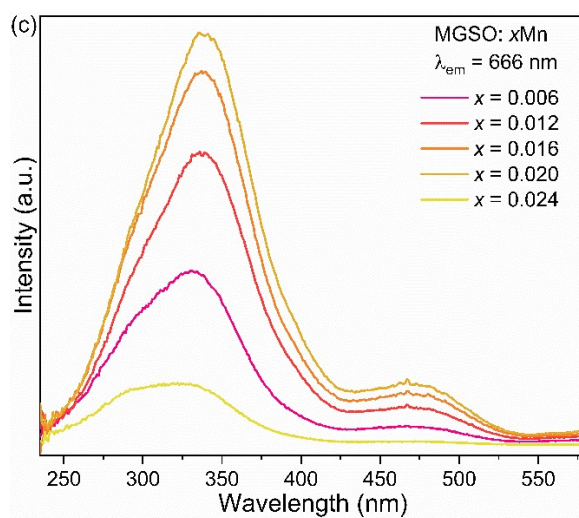
Figure S10. PLE spectra of MISO:*x*Mn monitored at wavelengths of 504 nm (a), 712 (b) and 666 nm (c).
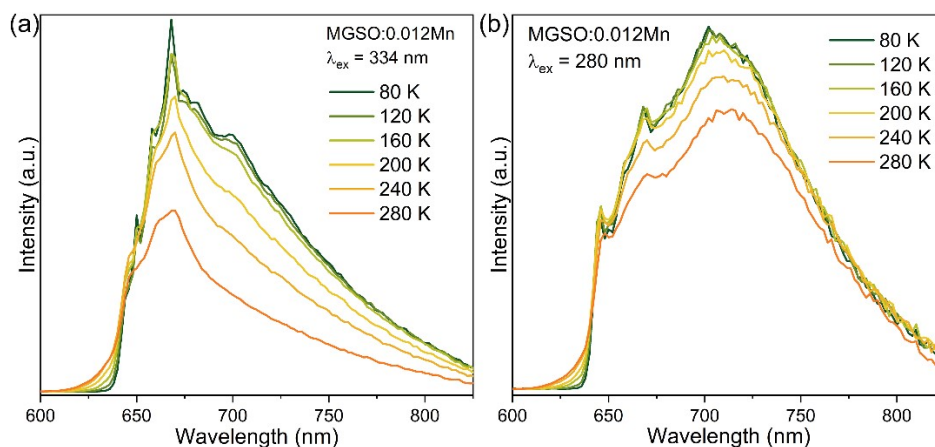
Fig. S11 Low-temperature PL spectra for MGSO:0.012Mn recorded under excitation wavelengths of 334 (a) and 280 nm (b).
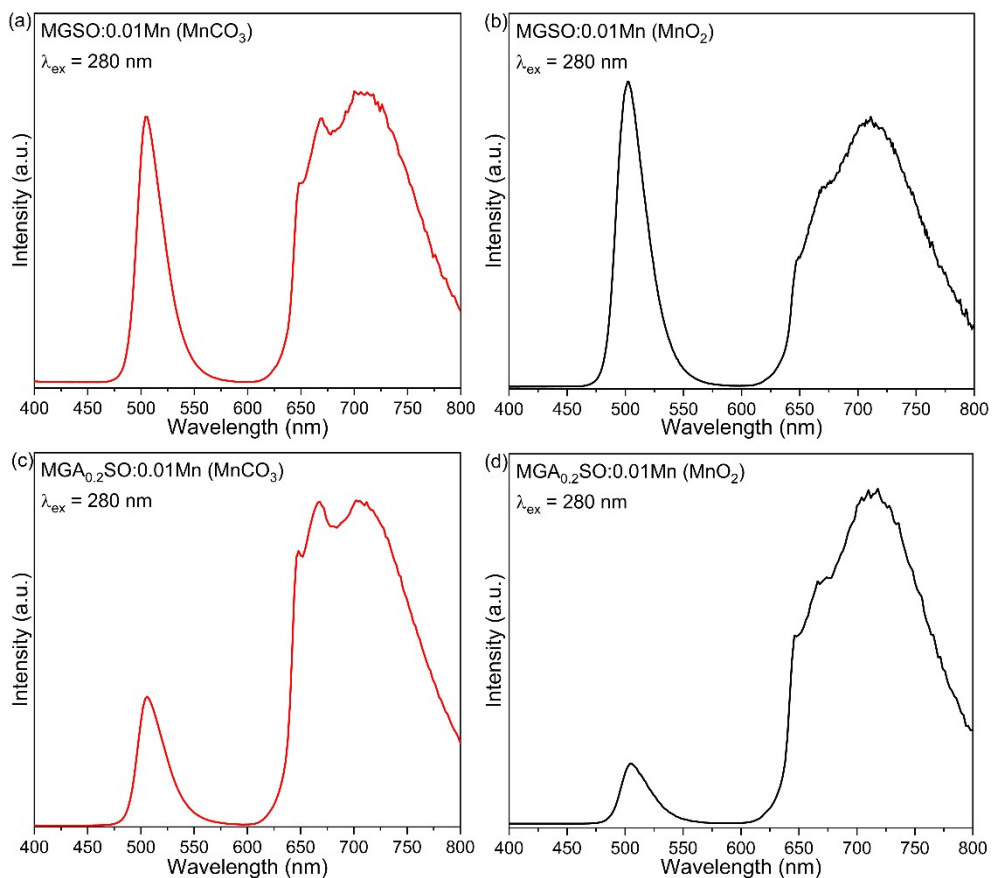
Fig. S12 Spectroscopic comparison for MGA$_y$SO:0.01Mn (y = 0 and 0.2) prepared with different Mn-sources.
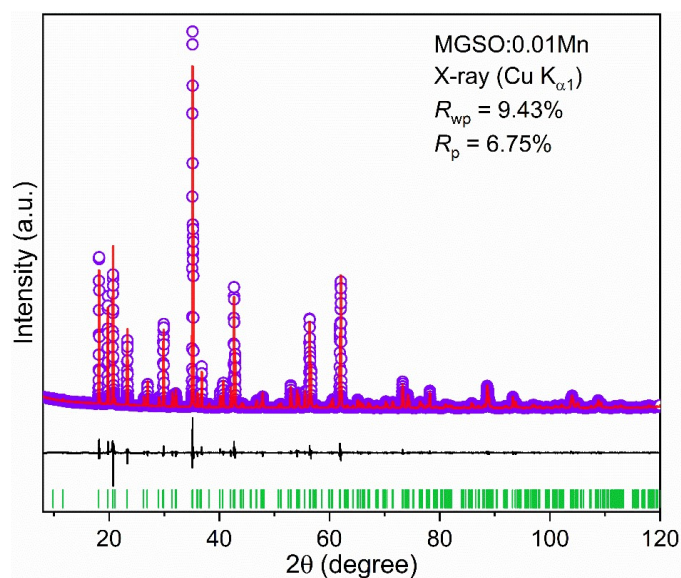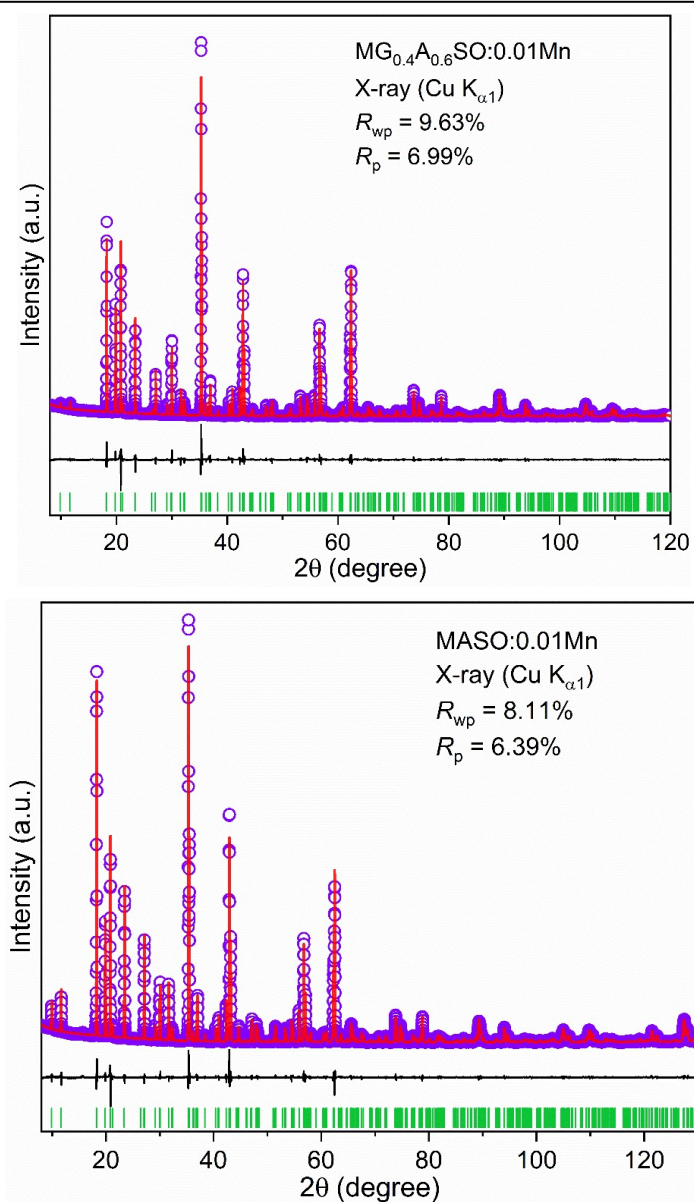
Fig. S13 Rietveld plots of XRPD data for MGA$_y$SO:0.01Mn with y = 0, 0.6, and 1.
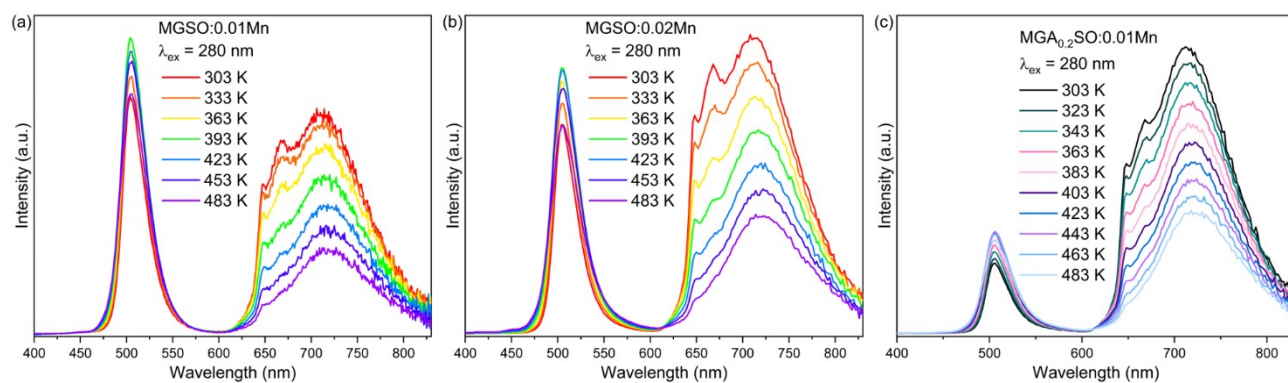
Fig. S14 Temperature-dependent PL spectra for MGSO:0.01Mn (a), MGSO:0.02Mn (b), and MGA0.2SO:0.01Mn (c) under an excitation wavelength of 280 nm.
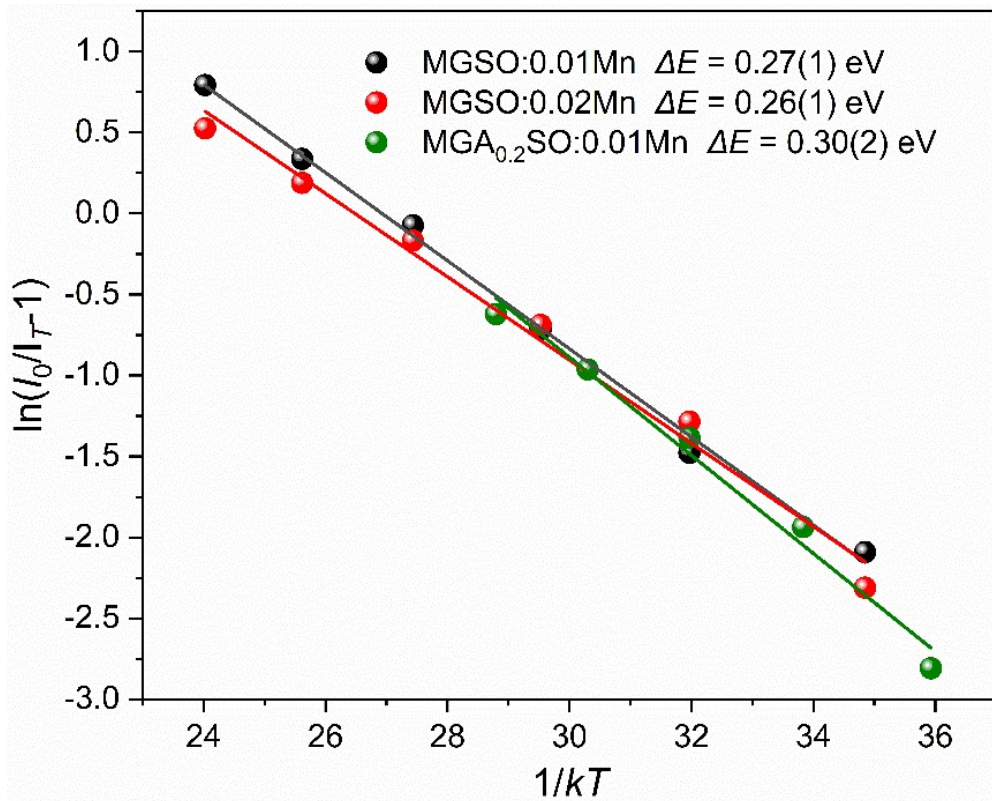
Fig. S15 Linear fitting of the $\ln(I_0/I_T - 1)$─$1/kT$ curves for MGSO:xMn (x = 0.01 and 0.02) and MGA$_{0.2}$SO:0.01Mn.
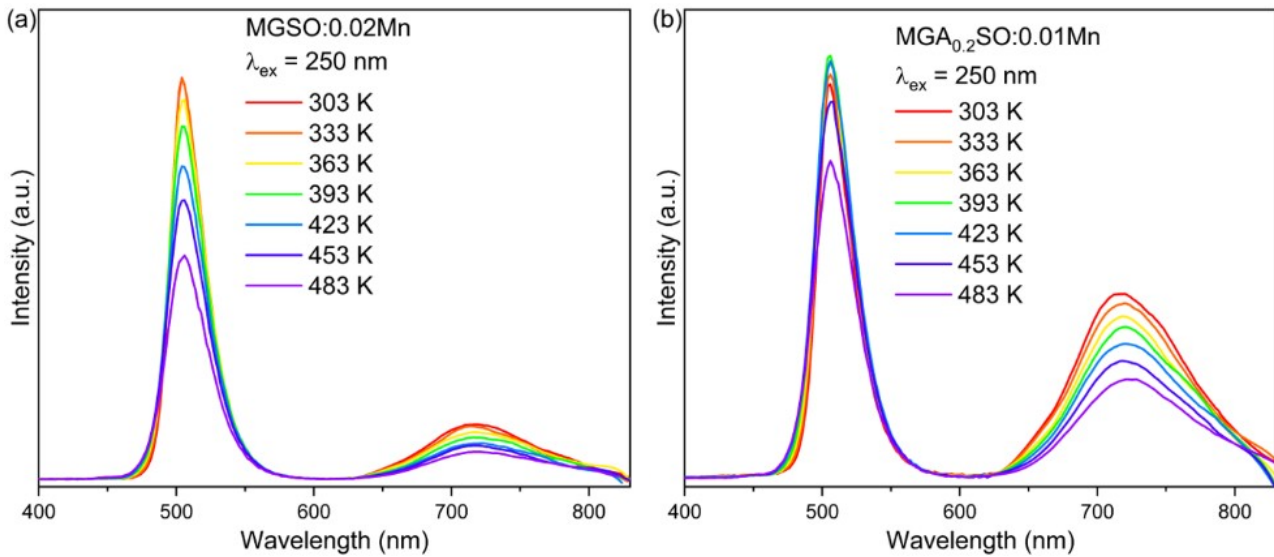
Fig. S16 Temperature-dependent PL spectra for MGSO:0.02Mn (a), MGA0.2SO:0.01Mn (b), and MGA0.4SO:0.01Mn under an excitation wavelength of 250 nm.
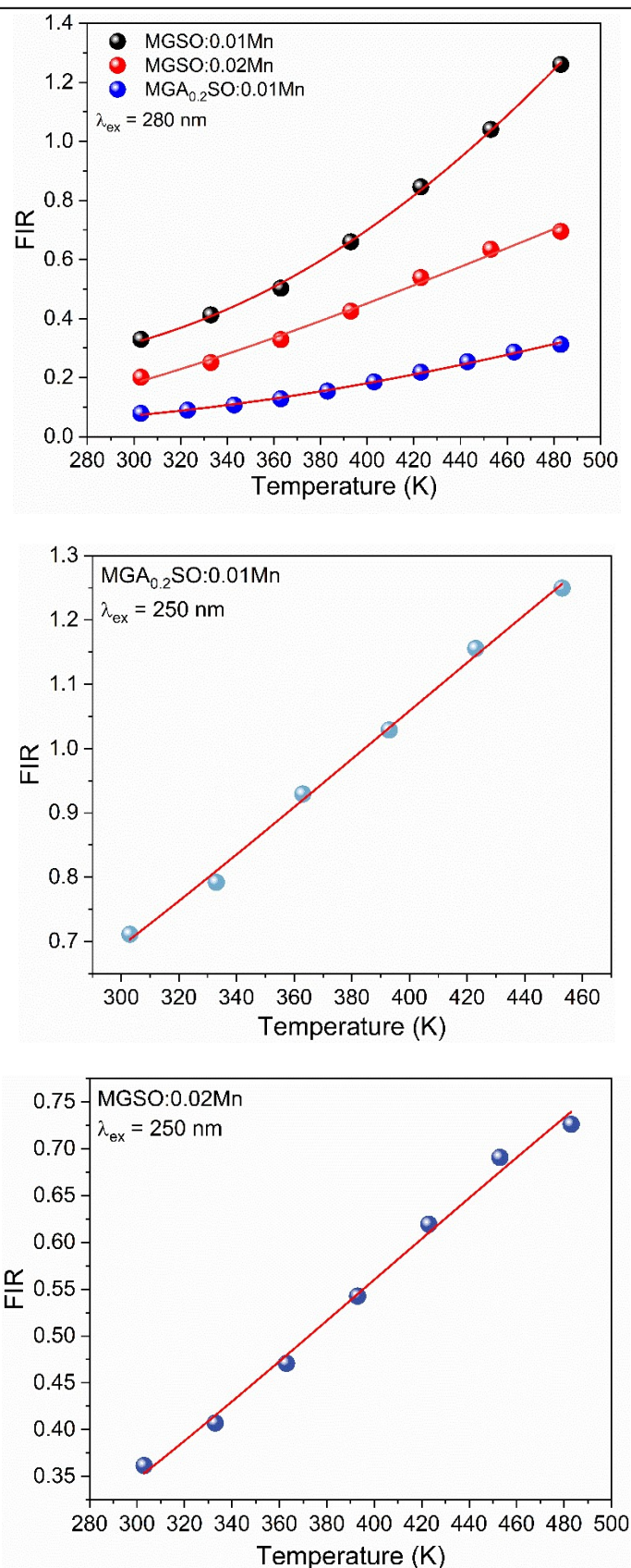
Fig. S17 Fitting of the FIR─T curves for MGSO:*x*Mn (*x* = 0.01 and 0.02) and MGA$_{0.2}$SO:0.01Mn.

Table S1. Crystallographic data for $MG_{0.5}A_{0.5}SO$.

formula	$Mg_4Ga_{0.5}Al_{0.5}SbO_8$	
source	X-ray (Cu Kα1)	neutron
temperature	298	
wavelength (Å)	1.5406	1.6220
space group (no.)	*Imma* (no. 74)	
a (Å)	5.98102(5)	
b (Å)	17.933(3)	
c (Å)	8.41505(6)	
V (Å^3)	902.66(1)	
Z	6	
d-spacing (Å)	0.82−10	0.81−10
R_{wp} (%)	9.79	5.20
R_p (%)	7.25	3.69
R_{exp} (%)	2.21	2.61
gof	4.43	1.99

Table S2. Atomic coordinates, site occupation factors, isotropic thermal displacement factors, of $MG_{0.5}A_{0.5}SO$ and MASO obtained from combined Rietveld refinements against both X-ray and neutron diffraction data.

			$MG_{0.5}A_{0.5}SO$			
atom	site	x	y	z	*sof.*	$B_{iso.}$ (Å^2)
Mg1/Al	8h	0	0.1691(1)	0.0006(3)	0.96(5)/0.04(5)	0.22(3)

Mg2/Al	8g	0.25	0.0095(7)	0.25	0.82(5)/0.18(5)	0.28(5)
Sb1	4b	0	0	0	1	1.5(2)
Sb2/Mg	4c	0.25	0.25	0.75	0.5/0.5	0.49(2)
Ga1/Al	4e	0	0.25	0.375 (2)	0.695(3)/0.305(3)	1.1(1)
Mg3/Ga	8h	0	0.0834(1)	0.6290(5)	0.973(2)/0.027(2)	0.62(4)
O1	8i	0.239(2)	0.25	0.511(2)	1	1.1(2)
O2	8h	0	0.1726(2)	0.2500(6)	1	0.4(1)
O3	8h	0	0.6663(4)	0.2640(7)	1	0.7(2)
O4	8h	0	0	0.2702(6)	1	0.7(2)
O5	16j	0.7889(5)	0.5816(1)	0.4915(6)	1	0.4(1)

MASO

atom	site	x	y	z	sof.	$B_{iso.}$ (Å^2)
Mg1	8h	0	0.16983(6)	0.0097(2)	1	0.28(3)
Mg2/Al	8g	0.25	0.09055(7)	0.25	0.75/0.25	0.58(3)
Sb1	4b	0	0	0	1	0.246(7)
Sb2/Mg	4c	0.25	0.25	0.75	0.5/0.5	0.57(1)
Al1	4e	0	0.25	0.3756(3)	1	0.44(3)
Mg3	8h	0	0.08341(8)	0.627(2)	1	0.35(2)
O1	8i	0.2534(8)	0.25	0.504(1)	1	1.1(1)
O2	8h	0	0.1670(4)	0.2576(8)	1	0.9(1)
O3	8h	0	0.6735(3)	0.2613(7)	1	0.42(8)
O4	8h	0	0	0.2370(8)	1	0.57(8)

O5	16j	0.7806(4)	0.5796(2)	0.4902(6)	1	0.37(5)

Table S3. Selected interatomic distances for MGSO, MG$_{0.5}$A$_{0.5}$SO and MASO.

MGSO

Mg1/Ga─O1 × 2	2.04(1)	Mg2/Ga─O2 × 2	2.06(1)	Mg3/Ga─O4	1.82(2)
Mg1/Ga─O3	2.06(3)	Mg2/Ga─O5 × 2	2.063(9)	Mg3/Ga─O3	2.02(2)
Mg1/Ga─O2	2.09(2)	Mg2/Ga─O4 × 2	2.189(9)	Mg3/Ga─O5 × 2	2.05(1)
Mg1/Ga─O5 × 2	2.09(1)	<Mg2/Ga─O>	2.104(9)	<Mg3/Ga─O>	1.99(2)
< Mg1/Ga─O>	2.07(2)				
Sb1─O4 × 2	1.96(2)	Sb2/Mg─O3 × 4	2.04(1)	Ga1/Mg─O2 × 2	1.80(1)
Sb1─O5 × 4	1.958(9)	Sb1/Mg─O1 × 2	2.07(2)	Ga1/Mg─O1 × 2	1.95(2)
<Sb1─O>	1.96(2)	<Sb1/Mg─O>	2.05(1)	<Ga1/Mg─O>	1.88(2)

MG$_{0.5}$A$_{0.5}$SO

Mg1/Al─O1 × 2	2.020(3)	Mg2/Al─O2 × 2	2.109(4)	Mg3─O4	1.910(4)
Mg1/Al─O3	2.042(7)	Mg2/Al─O5 × 2	2.051(5)	Mg3─O3	1.872(7)
Mg1/Al─O2	2.091(6)	Mg2/Al─O4 × 2	2.203(2)	Mg3─O5 × 2	2.080(4)
Mg1/Al─O5 × 2	2.015(3)	<Mg2/Al─O>	2.121(4)	<Mg3─O>	1.986(4)
< Mg1/Al─O>	2.034(4)				
Sb1─O4 × 2	1.934(5)	Sb2/Mg─O3 × 4	2.122(4)	Ga1/Al─O2 × 2	1.740(5)
Sb1─O5 × 4	1.934(3)	Sb1/Mg─O1 × 2	2.093(4)	Ga1/Al─O1 × 2	1.911(5)
<Sb1─O>	1.934(4)	<Sb1/Mg─O>	2.112(4)	<Ga1/Mg─O>	1.826(5)

MASO

Mg1─O1 × 2	2.062(2)	Mg2/Al─O2 × 2	2.060(2)	Mg3─O4	1.894(2)

Mg1—O3	2.066(4)	Mg2/Al—O5 × 2	2.009(3)	Mg3—O3	1.954(4)
Mg1—O2	2.091(4)	Mg2/Al—O4 × 2	2.203(1)	Mg3—O5 × 2	2.039(2)
Mg1—O5 × 2	2.050(2)	<Mg2/Al—O>	2.091(2)	<Mg3—O>	1.982(3)
< Mg1—O>	2.064(3)				
Sb1—O4 × 2	1.959(3)	Sb2/Mg—O3 × 4	2.041(2)	Al1—O2 × 2	1.728(3)
Sb1—O5 × 4	1.952(2)	Sb1/Mg—O1 × 2	2.053(4)	Al1—O1 × 2	1.851(3)
<Sb1—O>	1.954(2)	<Sb1/Mg—O>	2.045(3)	<Ga1/Mg—O>	1.790(3)

Table S4. Lattice parameters of the structures after DFT optimization.

Compounds	a (Å)	b (Å)	c (Å)	V (Å^3)
MGSO	6.07	18.23	8.55	947.14
MASO	6.03	18.06	8.46	921.77

Table S5. Fitted values of τ_1, τ_2, A_1, and A_2 for the decay curves of MGSO:xMn phosphors.

λ_{ex} = 252 nm, λ_{em} = 504 nm				
MISO:xMn	τ_1 ($\times 10^6$ ns)	τ_2 ($\times 10^6$ ns)	A_1	A_2
x = 0.006	0.8(1)	3.46(8)	79.(1)	850.(7)
x = 0.012	0.97(5)	3.17(9)	19(7)	74(2)
x = 0.016	0.26(7)	2.81(2)	148.(8)	793.(3)
x = 0.020	0.58(4)	2.79(6)	221.(8)	743.(2)
x = 0.024	0.52(9)	2.63(9)	229.(7)	673.(1)

Table S6. Fitted values of A, B, and ΔE for the FIR—T curves of MGSO:xMn (x = 0.01 and 0.02) and MGA$_{0.2}$SO:0.01Mn.

	A	B	ΔE
MGSO:0.01Mn (λ_{ex} = 280 nm)	0.21(2)	42.3(1)	0.153(8)
MGSO:0.02Mn (λ_{ex} = 280 nm)	-0.017(8)	6.2(8)	0.09(2)
MGA$_{0.2}$SO:0.01Mn (λ_{ex} = 280 nm)	0.03(1)	6.5(6)	0.13(1)
MGSO:0.02Mn (λ_{ex} = 250 nm)	0.123(8)	3.24(9)	0.07(2)
MGA$_{0.2}$SO:0.01Mn (λ_{ex} = 250 nm)	0.302(6)	5.50(8)	0.07(2)

Table S7. Rietveld refinement parameters, agreement factors, and calculated Debye temperatures for MGA$_y$SO:0.01Mn (y = 0, 0.6, 1.0).

y	a (Å)	b (Å)	c (Å)	V (Å)	R_{wp} (%)	R_p (%)	χ^2	Θ_D (K)[a]
0	5.9967(5)	17.986(8)	8.4442(9)	910.8(2)	9.43	6.75	4.44	739.6(9)
0.6	5.9681(3)	17.903(6)	8.4011(2)	897.6(7)	9.63	6.99	4.23	915.5(6)
1	5.9618(3)	17.870(9)	8.3839(4)	893.2(5)	8.11	6.39	3.53	1688.5(2)

[a] Debye temperature (Θ_D) is calculated according to the expression $\Theta_D = \sqrt{\dfrac{3\hbar^2 T N_A}{A_i K_B U_{iso,i}}}$, where U_{iso} indicates the atomic average displacement factor, and A_i is the atomic weight of the atom.